Niobium Incorporation into $CsPbI_2Br$ for Stable and Efficient All-Inorganic Perovskite Solar Cells

Zhanglin Guo[1], Shuai Zhao[2], Anmin Liu[3], Yusuke Kamata[1], Siowhwa Teo[1], Shuzhang Yang[1], Zhenhua Xu[1], Shuzi Hayase[1], Tingli Ma[1,4*]

[1]Graduate School of Life Science and Systems Engineering, Kyushu Institute of Technology, Kitakyushu, Fukuoka, 808-0196, Japan

[2]Chongqing Key Laboratory of Green Energy Materials Technology and Systems, College of Science, Chongqing University of Technology, Chongqing, 400054, P. R. China

[3]School of Petroleum and Chemical Engineering, Dalian University of Technology, Panjin Campus, Panjin, 124221, P. R. China

[4]Department of Materials Science and Engineering, China Jiliang University, Hangzhou, 310018, P. R. China

(* Correspondence: tinglima@life.kyutech.ac.jp)

Keywords

All-inorganic perovskite; $CsPbI_2Br$; Niobium doping; Phase stability; Carbon electrode

Abstract

All-inorganic perovskites are attracting increasing attention due to their superior thermal stability than that of the traditional $CH_3NH_3PbI_3$. While their inferior phase stability in ambient conditions is still an unsolved issue. Here, for the first time, we report the incorporation of niobium (Nb^{5+}) ions into the $CsPbI_2Br$ perovskite. Results indicate that Nb^{5+} can effectively stabilize the photoactive α-$CsPbI_2Br$ phase by the possible substitution of Pb^{2+}. With 0.5% Nb doping, the carbon electrode based all-inorganic perovskite solar cells achieved a high PCE of 10.42%, 15% higher than that of the control device. The Nb^{5+} incorporation reduces the charge recombination in the perovskite, leading to a champion V_{oc} of 1.27 V and negligible hysteresis effect. This work explicates the high compatibility of all-inorganic perovskite materials and unlocks the opportunities for the use of high-valence ions for perovskite property modification.

Introduction

Organic-inorganic hybrid perovskite solar cells (PSCs) have been attracting tremendous attention and have experienced high-speed development in photoconversion efficiency (PCE) in recent years.[1-2] The organic components, such as methylammonium (MA^+) and formamidinium (FA^+), are very favorable in forming high-quality perovskite films with high PCEs.[3] While the MA^+ and FA^+ are volatile at the temperature of 80 and 100

^{o}C,[4-5] respectively, which causes the perovskite thermal unstable and consequently reduces the lifetime of the PSCs. Incorporating Cs^{+} or completely replacing MA^{+} and FA^{+} with Cs^{+} is a promising approach to solve the issue because Cs based perovskites are extremely stable at high temperatures.[6] However, the Cs based perovskites possess an inevitable disadvantage where the photo-active black α-phase is unstable at room-temperature and very easily transforms to photo-non-active yellow δ-phase.[7-8] Therefore, it is an important topic to stabilize the black phase at room-temperature in ambient conditions. Apart from reducing the crystal size and increasing the crystal strain etc.,[9-10] there are two main strategies to stabilize the black phase of inorganic perovskites.

One approach is incorporating Br^{-} into the perovskite structure because Br^{-} has a smaller ionic radius of 1.96 Å than I^{-} of 2.20 Å.[11] When Br^{-} is used as X ion in ABX_3 perovskite, the size of $[BX_6]^{4-}$ octahedral and the formed cubooctahedral voids for the Cs cation will be reduced, which promises larger Goldschmidt tolerance factor (τ) and more stable cubic perovskite phase.[12] However, Br^{-} incorporation will simultaneously enlarge the band gap of the perovskite, which is undesirable for light absorption. For balancing the photovoltaic performance and the structure stability, $CsPbI_2Br$ is a fine choice due to its proper band gap (1.90 eV) and higher phase stability than that of $CsPbI_3$.[13]

The other way is substituting (doping and alloying) Pb^{2+} ions with smaller metal ions, also for reducing the $[BX_6]$ size. Up to now, various kinds of metals have been introduced into the perovskite materials, such as divalent ions Ca^{2+}, Mn^{2+}, Sn^{2+}, Sr^{2+}, Zn^{2+} and trivalent ions Sb^{3+}, Bi^{3+}, Eu^{3+}, and some other lanthanide ions.[12-14] These foreign ions have been proved to be efficient in increasing the stability of the black α-phase and enhancing/maintaining the performance of the resultant devices. While only the metal ions possessing similar valence state with Pb^{2+} have been selected as dopants and the possibility of incorporating metals ions with higher valences into the perovskite is still unknown. Niobium (Nb) is a widely used element for doping conventional perovskite oxides ($BaTiO_3$, $BiFeO_3$, etc.) for modifying the microstructure, ferroelectric and piezoelectric properties, in which the Nb^{5+} ions will partly replace the B site atoms of perovskite.[15] Recently, Nb^{5+} has been used as a dopant for TiO_2 layer in PSCs and enhanced performance was achieved.[16] While there are rare reports on trying to introduce the Nb^{5+} ions into the light absorption layer. During the preparation of this manuscript, a study was published, in which the NbF_5 was used as an additive to stabilize the α-phase of FA-based perovskite

materials.[17] Thus it is worth trying to incorporate Nb into the inorganic halide lead perovskite and to study its effect on the perovskite phase stability and the device performance.

In this paper, we incorporated Nb^{5+} into the $CsPbI_2Br$ perovskite and investigated its effect on the perovskite phase stability and photovoltaic performances. Results indicate that the introduction of Nb^{5+} can effectively stabilize the black α-phase of the $CsPbI_2Br$ perovskite at room-temperature in ambient condition, and higher Nb^{5+} concentration leads to a longer lifetime of black α-phase. Moreover, Nb^{5+} doping enhances the performance and reduces the hysteresis of the all-inorganic PSCs. The theoretical calculation was also adopted to realize the impact of Nb doping on the electronic properties of the perovskite. We believe this first work on pentavalent ion doping into the all-inorganic perovskite will bring deeper understanding of the mechanism of foreign metal ion incorporation in perovskite and unlock more opportunities for perovskite property modification.

Results and discussion

Different amount of Nb^{5+} (0.25 to 4 mol%) were introduced into the $CsPbI_2Br$ by adding a certain amount of 0.2 M $NbCl_5$ stock solution into 1.0 M CsBr and PbI_2 solution (check specific details in the supporting information). The obtained solutions after mixing for several hours are shown in Figure S1. It is interesting that the color of the perovskite precursors turns into darker brown with increasing the amount of $NbCl_5$, though the $NbCl_5$ and $CsPbI_2Br$ solution are transparent and yellow in color, respectively. The color change is hypothesized to be attributed to the interaction between Nb^{5+} and the perovskite precursor, rather than the Cl^- from $NbCl_5$.[9, 18] Moreover, there was no precipitate formed for Nb^{5+} containing solutions even stored for longer than one month, indicating homogeneous and stable properties.

The precursor was spin-coated on the passivated SnO_2 film,[19] followed by a two-step annealing process. Specifically, the film was annealed at 40 ºC for several minutes to make the film vary from transparent to light brown and then 160 ºC to get a dark brown film. The first low-temperature annealing is for the mild solvent evaporation and the phase transition (from amorphous to main black α-phase).[20-21] In our experiments, for the control $CsPbI_2Br$ film, the optimized annealing time at 40 ºC is 4 min since longer time will form blurry film and shorter annealing time will result in a low coverage film due to inefficient mass transfer. In addition, it should be noted that the optimal 40 ºC annealing time for the Nb incorporated films decreases with higher Nb incorporation. For example, the proper annealing time at 40 ºC for the perovskite film with 0.5 mol% Nb^{5+} is 3 min. This might

because the solutions with Nb have lower viscosity, and the Nb ions promote the nucleation and the phase transition process.[22]

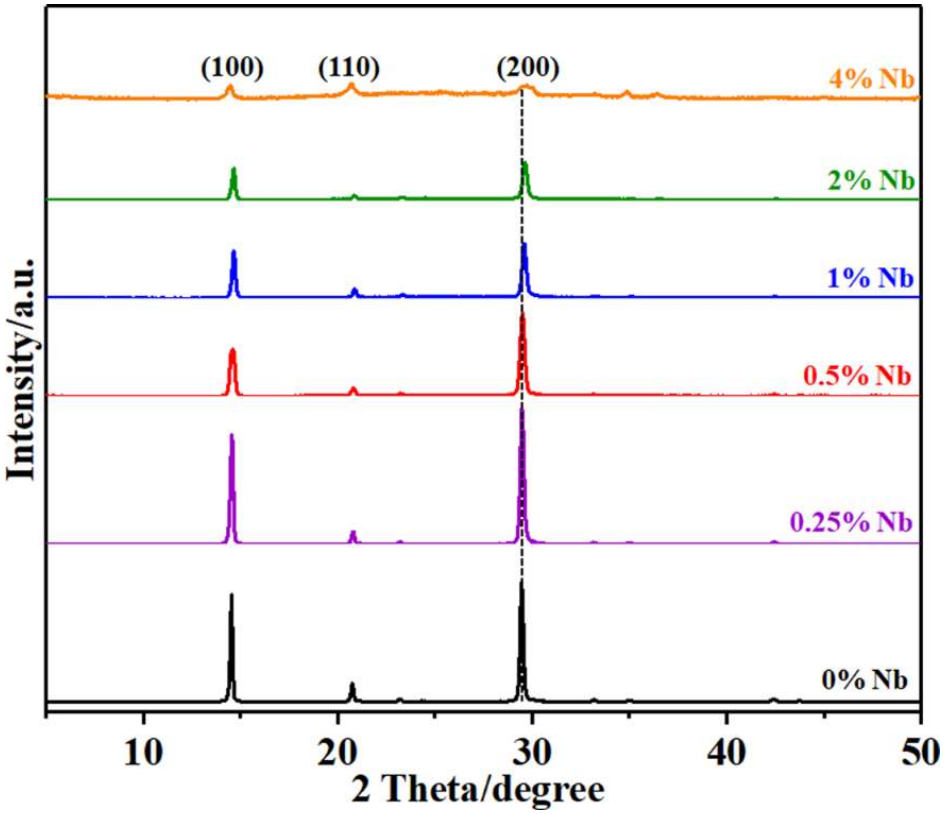

Figure 1 XRD patterns of $CsPbI_2Br$ films with different amount of Nb.

The XRD patterns of the samples after 160 ºC annealing for 10 min are shown in Figure 1. The peaks at 14.6°, 20.8°, and 29.5° are assigned to (100), (110), and (200) crystal face of cubic $CsPbI_2Br$, respectively, which indicate that all the as-prepared samples are pure cubic $CsPbI_2Br$ phase without any impurity.[23]

Table 1 Parameters derived from the XRD patterns of $CsPbI_2Br$ films with different amount of Nb.

Nb content (%)	Main peak position (º)	FWHM (main peak)	d-spacing (nm)	Lattice constant (nm)	Lattice strain (%)
0	29.44	0.164	0.3031	0.6062	0.080
0.25	29.48	0.214	0.3028	0.6056	0.085
0.5	29.49	0.247	0.3027	0.6054	0.098
1	29.55	0.253	0.3021	0.6041	0.140
2	29.61	0.266	0.3014	0.6029	0.210
4	29.70	0.643	0.3006	0.6012	0.287

While there are some differences between the samples. Firstly, the main peak at around 29.5° shifts to higher angle with increasing the amount of Nb^{5+}. The peak positions and the d spacing values are summarized in Table 1. Clearly, the d spacing reduces when the Nb^{5+} amount increases. Secondly, the peak intensities reduce and the FWHM values enlarge with the Nb^{5+} adding amount increasing, meaning lower crystallinity. Therefore, the foreign Nb ions have a great effect on the crystallization process of the perovskite film.

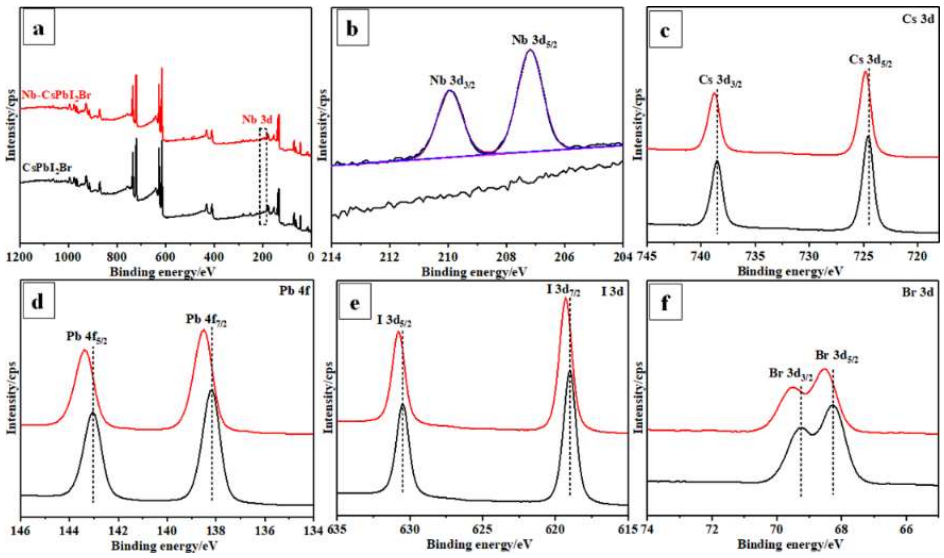

Figure 2 XPS spectra of pure (black line) and 4% incorported (red line) $CsPbI_2Br$ films: (a) survey spectra; (b) Nb 3d; (c) Cs 3d; (d) Pb 4f (e) I 3d; (f) Br 3d.

Figure 2 shows the XPS spectra of the pure $CsPbI_2Br$ and 4% Nb incorporated $CsPbI_2Br$ films. The presence of Nb^{5+} is evidenced through the explication of two binding energy peaks at around 200 eV, attributing to the Nb 3d core levels, which are not found in the pure sample (Figure 2a). Specifically, the two binding energy peaks at 209.9 and 207.2 eV (Figure 2b) are corresponding to Nb $3d_{3/2}$ and Nb $3d_{5/2}$, respectively.[16] Thus we can confirm that the Nb^{5+} was introduced into the perovskite film. Figure 2c-f show the XPS spectra of the Cs, Pb, I and Br elements, respectively. Notably, all the peaks of the Nb incorporated $CsPbI_2Br$ shift obviously compared with the pure film without Nb. The C1s peaks of the two samples (Figure S2) are at almost the same positions, indicative of the same measurement conditions. Thus, the shift of the elements should be attributed to the effect of Nb^{5+} rather than test error. The Nb should be located within the perovskite lattice because simple physical mixing of the elements could not lead to any remarkable chemical state changes and XPS peak shifts for all the elements.[22, 24-25] The theoretical study predicted that niobium trend to occupy the B site of the halide perovskite.[26] If so, partial

replacing Pb^{2+} (1.19 Å) with the smaller Nb^{5+} (0.64 Å) will lead to the contraction of [BX_6] and the changes in chemical bonding properties, which is reflected by the shift of XPS peaks for all the elements.[24] Moreover, the energy-dispersive X-ray spectroscopy (EDX) elemental maps in Figure S3 indicate that Nb is uniformly distributed in the sample.

The lattice constants obtained from the XRD patterns of the perovskite films are shown in Table 1. We can find that the lattice constant decreases with increasing Nb amount. Previous publications reported that the lattice increases if the foreign ions exist at the interstitial positions,[22] which is different from that of ours. Therefore, based on the variations including the reduction in lattice constants, XPS peak shifts for all elements and uniform Nb element dispersion, Nb ions are speculated to occupy the Pb positions.

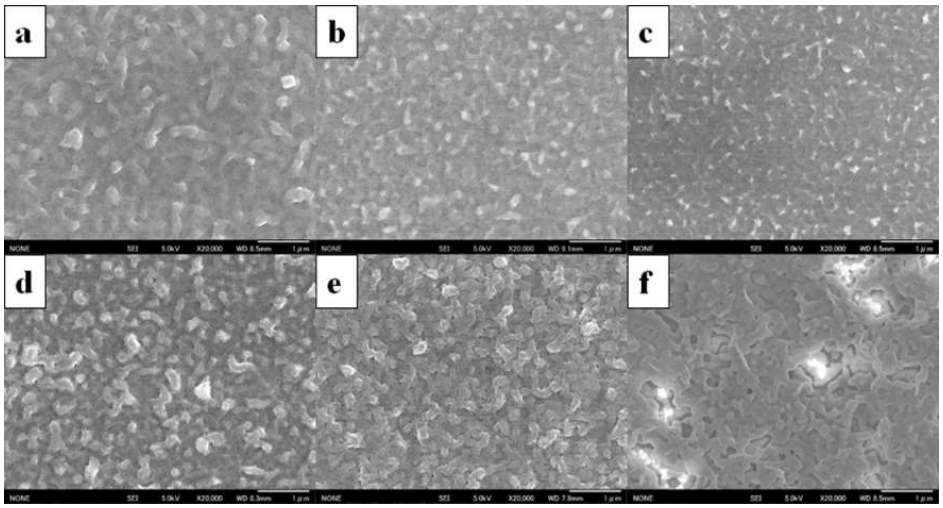

Figure 3 SEM images of $CsPbI_2Br$ films with different amount of Nb doping: (a) 0%; (b) 0.25%; (c) 0.5%; (d) 1%; (e) 2%; (f) 4%.

The SEM images of the samples with different amount of Nb are shown in Figure 3. The control perovskite film obtained by the two-step annealing process has a dense morphology without pinholes, which is promising for suppressing recombination of charges. The grain boundaries are not very clear because the anti-solvent was not used in our film preparation process, consistent with the other reports.[27-28] There are several branches on the film surface, meaning a non-uniform morphology, similar with that of the previous report.[24] When 0.25% amount Nb was introduced into the perovskite, there are no obvious changes except that the branches disappeared. With 0.5% amount Nb incorporation, the film grew smoother and the crystal size became smaller and more uniform than that of the film without Nb. This might be attributed to the lower viscosity of the solution with Nb for better mass

transfer and the role of Nb in promoting the nucleation process. The smaller crystal size means low crystallinity, in accordance with the XRD peak intensity reduction and FWHM enlargement. The smoother surface is beneficial for the contact between the perovskite and the carbon electrode.[29] While further increasing the amount of Nb doping makes the films rougher and non-uniform. For example, the film of 2% Nb has a rough surface with pinholes. The film with 4% Nb shows some independent white particles, which could be the segregation of excess $NbCl_5$ out of the perovskite grains.[9] To some extent, these segregated particles hinder the perovskite crystal growth and result in low-crystallinity films. Therefore, the film with 4% Nb has the lowest crystallinity and the lowest XRD peaks.

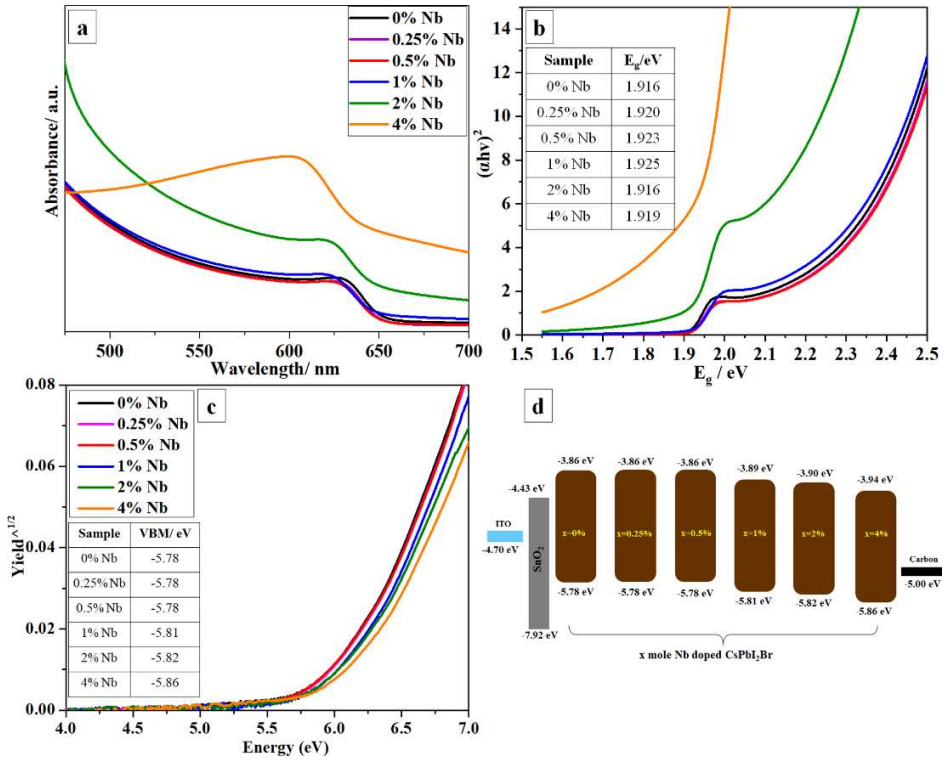

Figure 4 (a) UV-vis spectra, (b) tauc plots, (c) PYS spectra and (d) the resultant energy band structure of $CsPbI_2Br$ films with different amount of Nb doping, and the energy alignment for the components of the device.

It is accepted that the light absorption properties of the film are highly dependent on the film feature. From the UV-vis spectra (Figure 4a), we can find that the samples with low doping amount (less than 1%) have almost the same light absorption ability with that of the control sample, except a slight blue shift at the absorption edge. Obvious differences are observed when the doping amount is further improved to 2% and 4%: where the

absorbance intensities become stronger. The main reason might be the rough feature of the two samples, as can be observed in Figure 6a. When increasing the film surface roughness, the amount of absorbed light will increase because of the decreasing in the back-reflection of light. The band gaps of the materials were calculated by the tauc plots transformed from the UV-vis absorption spectra (Figure 4b). The corresponding values were summarized in the Table inserted in Figure 4b, where we can see that all the samples possess almost the same band gap. In addition, the band structures of the samples were investigated through the photoelectron yield spectroscopy (PYS), as shown in Figure 4c. The valence band maximum (VBM) values were obtained from the PYS results, and the corresponding conduction band minimum (CBM) were calculated by combining the VBM and the band gaps, as shown in Figure 4d. We can find that the minute amount of Nb doping has no effect on the band structure, while the VBM and CBM plunge when more than 1% amount of Nb is incorporated. The 4% Nb doping results the most obvious change with the lowest VBM and CBM positions. Therefore, the band structure changes more obviously with more amount of Nb.

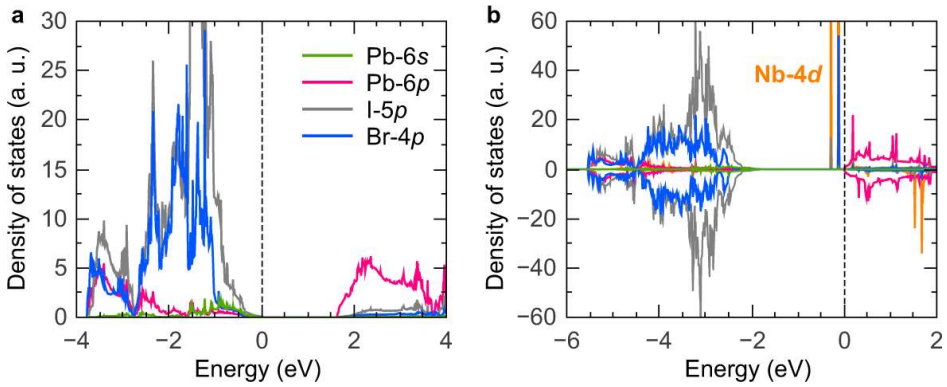

Figure 5 Partial density of states for (a) $CsPbI_2Br$ and (b) $CsPb_{0.875}Nb_{0.125}I_2Br$ calculated by GGA method. The Fermi energy level was set to zero.

To investigate the electronic properties of Nb-doped $CsPbI_2Br$, we calculated the partial density of states, which is shown in Figure 5. For the case of $CsPbI_2Br$, the valence bands maximum (VBM) is composed of I and Br *p*-orbitals with a small contribution from Pb 6*s*-orbitals, and the conduction bands minimum (CBM) mainly consists of the Pb 6*p*-orbitals. For the $CsPb_{0.875}Nb_{0.125}I_2Br$, the VBM exhibit similar electronic properties with $CsPbI_2Br$. After Nb substitution, the Nb 4*d*-orbitals split in different energy ranges respectively. Partial 4*d*-electrons of Nb localized on conduction bands at about 1.5 eV above the Fermi level in the spin-down channel. While in the spin-

up channel, the interaction between Nb 4*d* with I and Br *p*-orbitals forms intermediate bands slightly below the Fermi energy level. Due to the Nb 4*d* electrons, the Fermi level shifts up to the CBM, resulting in the n-type semiconductor feature of $CsPb_{0.875}Nb_{0.125}I_2Br$, which is similar to the Sb caused n-type doping for $CH_3NH_3PbI_3$.[30]

The excess positive charge caused by Nb^{5+} is possibly balanced by Pb^{2+} vacancies and excess anions at interstitial sites. The defect properties of Nb-doped $CsPbI_2Br$ were studied by calculation the formation energy E_{form} for different defect types (including Cs vacancy V_{Cs}, Pb vacancy V_{Pb}, and interstitial Cl defects I_{Cl}), according to the approximation: $E_{form} = E_{deficient} - E_{perfect} \pm E_X$. Here the $E_{perfect}$ and $E_{deficient}$ are energies of the perfect and deficient supercell structures, E_X is the energy of defect element, + corresponds to the vacancy and – is for the interstitial defect. The results are shown in Table S1. The negative values suggest that the formation of V_{Pb} and I_{Cl} are exothermic reactions. The E_{form} of V_{Pb} is predicted to be -5.20 eV, indicating the formation of Pb vacancies after Nb doping. In addition, the defect formation energy for I_{Cl} in the Nb-doped $CsPbI_2Br$ is also obviously smaller than that of the pristine $CsPbI_2Br$, indicating the possible existing of excess Cl anions at interstitial sites.

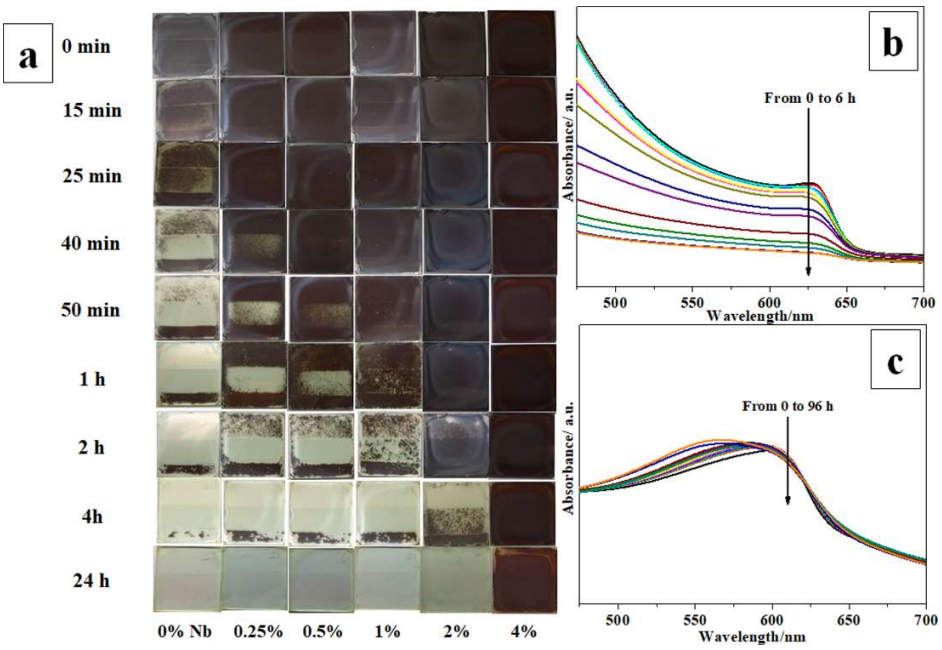

Figure 6 (a) Color variations of $CsPbI_2Br$ films with different amount of Nb doping. (test condition: ambient, 23 °C, RH=55%), and UV-vis spectra variations of (b) pure and (c) 4% Nb doped $CsPbI_2Br$ film. (test condition: ambient, 21 °C, RH=30%).

Figure 6a shows the photographs of $CsPbI_2Br$ films stored in ambient at the temperature of 23 °C and relative humidity (RH) of 55%. As observed, the color of the control sample faded in the first 15 min and the black α-

phase wholly changed to yellow δ-phase in the first one hour, as depicted by the XRD variations in Figure S4. When the Nb was doped into the perovskite, the black α-phase lasted for a longer time than that of the control one. For example, the film color of the 4% Nb doped perovskite remains the same even after 24 hours. We recorded the variations of the control and the 4% Nb incorporated film by UV-vis spectra, as shown in Figure 6b and c. When the films were stored in ambient at 21 ºC with the RH of 30%, the characteristic absorption edge of the α-$CsPbI_2Br$ film completely disappeared after 6 h, while the 4% Nb doped film has no changes even after 96 h. As a result, Nb can stabilize the α-$CsPbI_2Br$ phase at room temperature and the lifetime prolongs with increasing Nb doping amount.

When Nb occupies the B site of the $CsPbI_2Br$ crystal structure, its smaller size and more electron charge will decrease the $[BX_6]$ size and shrink the lattice, which makes the Cs match well with the cubooctahedral voids, thus stabilize the perovskite structure. This can be verified by the variations in Goldschmidt's tolerance factor (τ) as Equation (1):[31]

$$\tau = \frac{R_A + R_X}{\sqrt{2}(R_B + R_X)} \quad (1)$$

The R_A, R_B, and R_X represent the ionic radius of A-site cation, B-site cation, and X-site anion, respectively. The perovskite materials tend to form an orthorhombic structure when $\tau < 0.8$, cubic structure when $0.8 < \tau < 1$, and hexagonal structure when $\tau > 1$. Therefore, the bromine-based perovskite with smaller $[BX_6]$ octahedral size and larger tolerance factor, possesses better phase stability than that of the iodide perovskites (τ=0.807 for $CsPbI_3$ and 0.815 for $CsPbBr_3$). As for the mixed A-site, B-site, and mixed halide perovskite, the τ is calculated using effective ion size. For example, the effective halide size of $CsPbI_xBr_{3-x}$ can be calculated by Equation (2):[31]

$$R_{effective} = \frac{x}{3}R_{I^-} + \frac{3-x}{3}R_{Br^-} \quad (2)$$

The effective size of halide in $CsPbI_2Br$ is 2.12 Å and the τ is 0.810. Similarly, the effective size of B-site ion in Nb doped $CsNb_xPb_{1-x}I_2Br$ can be calculated by Equation (3):

$$R_{effective} = xR_{Nb^{5+}} + (1-x)R_{Pb^{2+}} \quad (3)$$

According to the above equations, we calculated and listed the τ of different amount Nb doped perovskite materials in Table S2. When 4% Nb was incorporated into the perovskite, the effective cation size of mixed Nb and Pb is 1.168 Å, resulting in a τ value of 0.815. Therefore, the perovskite with 4% Nb doping possesses the

highest stability. In addition, the lattice strain promotes the phase stability by causing distortion of cubic structure.[9, 18] We analyzed the lattice strain by refining the XRD patterns and the results are shown in Table 1. We found that the lattice strain increases with increasing the amount of Nb, which agrees with the stability gradient.

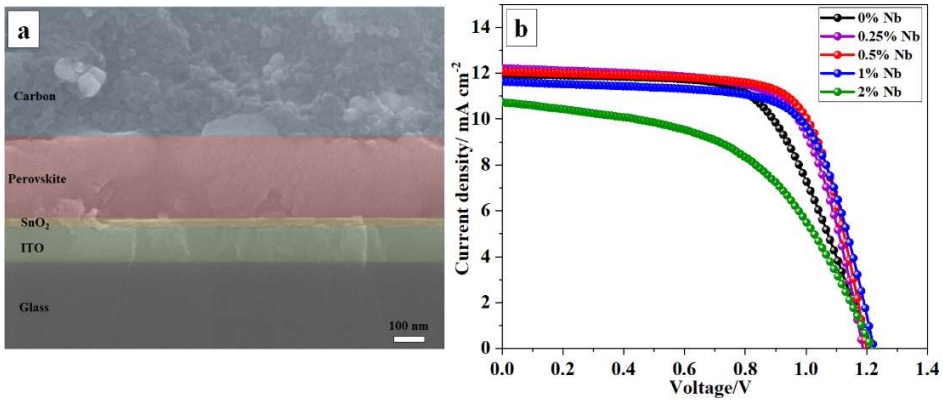

Figure 7 (a) Cross-sectional SEM image of carbon electrode based $CsPbI_2Br$ perovskite device and (b) J-V curves of the devices with different amount of Nb doping.

Table 2 Photovoltaic parameters of $CsPbI_2Br$ PSCs with different amount of Nb doping.

Sample	V_{oc}/V	J_{sc}/mA cm^{-2}	FF	PCE/%
0% Nb	1.21	11.95	0.63	9.05
0.25% Nb	1.18	12.22	0.69	9.94
0.5% Nb	1.20	12.06	0.72	10.42
1% Nb	1.22	11.63	0.69	9.84
2% Nb	1.21	10.73	0.52	6.69

In order to study the effect of Nb doping on the PSCs performances, we fabricated a carbon electrode based HTM-free device, as shown in the cross-sectional SEM image of the device (Figure 7a). The fabrication details of the carbon electrode are depicted in the SI. Figure 7b shows the current density-voltage (J-V) curves of the champion devices based on $CsPbI_2Br$ with different Nb doping amount. The corresponding photovoltaic parameters were summarized in Table 2. The device based on $CsPbI_2Br$ without dopant achieved a PCE of 9.05%, which is much higher than that of the literature (4.75%) with the same fabrication process, components and device structure.[27] For the Nb doped PSCs, the device gave the highest PCE of 10.42% when 0.5% Nb was added, high than ever-reported carbon based all-inorganic $CsPbI_2Br$ PSCs.[13] The J_{sc} value matches well with the calculated

value from the IPCE spectra (Figure S5a). The stability of output (SOP) of the reference and 0.5% Nb based device is shown in Figure S5b and c. Both the devices maintain high performances under continuous measurements for 120 s. The low J_{sc} of the devices with 2% amount Nb should be attributed to its lower film quality. The obvious increasing in FF was achieved with less than 2% Nb doping, which is the main reason for the device performance enhancement.

In order to verify the reproducibility of the device performances, we fabricated 18 cells for the reference and 0.5% Nb doped type. The detailed statistics of the photovoltaic parameters for the devices are presented in Figure S6 and summarized in Table S3. Results indicate that the J_{sc} values are very similar owing to their same optical properties. The average FF was enhanced from 0.60 to 0.70, which could be attributed to the uniform morphology and smooth surface that provides better contact with the carbon electrode.[32-33] The V_{oc} was enhanced from an average of 1.20 to 1.22 V, where the champion V_{oc} of 1.26 V was achieved for the reverse scan (RS) and 1.27 V for the forward scan (FS) when 0.5% Nb was doped into the $CsPbI_2Br$ perovskite (Figure S7). These V_{oc} values are higher than most of the $CsPbI_2Br$ based PSCs regardless of carbon or noble metal electrode. Finally, the average PCE was increased from 8.56% to 10.06% with 0.5% Nb doping.

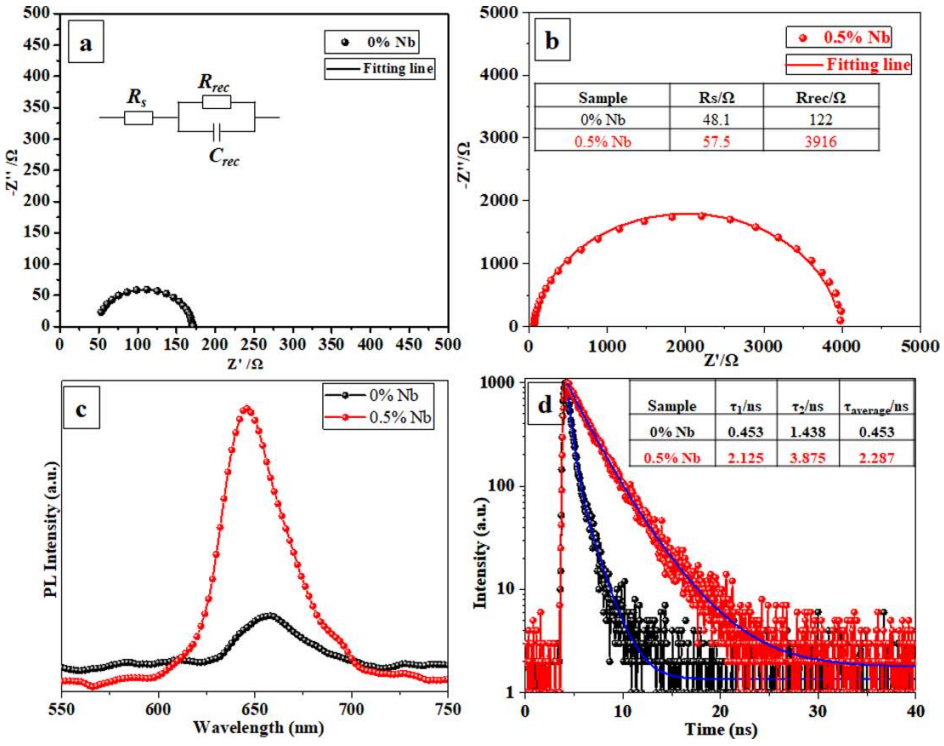

Figure 8 Nyquist plots of (a) 0 % and (b) 0.5% Nb doped $CsPbI_2Br$ based device, (c) PL and (d) TRPL spectra of 0 % and 0.5% Nb doped $CsPbI_2Br$ film.

The electrochemical impedance spectroscopy (EIS) measurements were carried out to investigate the charge transfer properties of the PSCs. The measurements were conducted at an applied bias of 0.6 V in dark condition and the results for the reference and 0.5% Nb based PSCs are shown in Figure 8a and b. The equivalent circuit and the fitting results are inserted in Figure 8a. In general, the high-frequency arc represents the transport process combining the transport resistance and the transport chemical capacitance, which are related to the series resistance (R_s) from the cathode to the anode. While the arc at the low-frequency region represents the recombination resistance (R_{rec}) and the chemical capacitance (C_{rec}) in the device.[34-35] The two samples have very similar R_s due to the same device structure. While the 0.5% Nb doped $CsPbI_2Br$ based device has much higher R_{rec} (3916 Ω) than that of the reference device (122 Ω), which implies that the recombination process in the former device is highly suppressed.[36] The highly increased recombination resistance is account for the high V_{oc} of 1.27 V. We also measured the EIS of other devices with different Nb doping amount, as shown in Figure S8 and Table S4. We found that after Nb incorporation, the devices possess larger R_{rec} than that of the control device. Thus the Nb doping can effectively suppress the charge recombination in PSCs.

To better understand the effect of Nb doping on the electron extraction and transport process, the steady-state photoluminescence (PL) and time-resolved photoluminescence (TRPL) measurements for the perovskite films were carried out. The results for the reference and 0.5% Nb doped film are shown in Figure 8c and d. It is obvious that the PL intensity sharply increases after 0.5% Nb incorporation, which is similar to that of Nb doping into FA-based perovskite materials.[17] It is generally believed that the higher PL intensity is associated with the fewer traps and defects in the perovskite layer.[37] Thus 0.5% Nb doping can significantly reduce the traps and defects in the perovskite film, meaning better film quality and promising for better performance.[38-39] Moreover, a blue shift in the PL spectra is observed with the maxima at 658 and 646 nm for 0% and 0.5% Nb, respectively. This is attributed to the reduction in crystallinity and grain size after 0.5% Nb incorporation.[10, 39] In contrast, the larger amount of Nb doped into the perovskite film induces lower film qualities with increased traps and defects, thus the blue shifts are not striking (Figure S9a). Figure 8d shows the TRPL spectra of the samples and the decay time (τ) is calculated via the double-exponential fits of Equation (4):

$$y = A1 * \exp\left(-\frac{x}{\tau 1}\right) + A2 * \exp\left(-\frac{x}{\tau 2}\right) + y0 \quad (4)$$

The former (τ_1) is resulted from the surface recombination process while the latter (τ_2) is attributed to the recombination process taken place in the grains.[40] The fitted parameters are listed in the Table inserted in Figure 8d. For the reference $CsPbI_2Br$ film, the PL lifetimes are 0.453 and 1.438 ns for τ_1 and τ_2, respectively. While the PL lifetime was prolonged to 2.125 and 3.875 ns for τ_1 and τ_2, respectively. As observed from Figure S9b, all the films with Nb doping (less than 2%) exhibited longer lifetime than the control film, indicative of the suppressed recombination process in the perovskite film,[41-42] which is consistent with the performances of the devices.

Hysteresis is commonly coming along with the photovoltaic performance measurements of PSCs, especially for the planar PSCs. We compared the hysteresis properties of the PSCs with different amount of Nb doping were compared by measuring the device in both reverse and forward scanning direction. The hysteresis index (HI) is defined as Equation (5):[43]

$$Hysteresis\ index = \frac{\mathrm{PCE_{reverse}} - \mathrm{PCE_{forward}}}{\mathrm{PCE_{reverse}}} \quad (5)$$

The device performances are shown in Figure S10 and the HI are summarized in Table S5. Results illustrate that the reference device without Nb has obvious hysteresis with the HI value of 18.99%. When a certain amount of Nb (less than 2%) is incorporated into the film, the hysteresis is effectively suppressed. Among the devices, the 0.5% Nb doped device has the smallest and negligible HI of 3.55%, owing to the reduced traps states by the proper amount of Nb doping,[44] as mentioned above. In contrast, the 2% Nb doped film based solar cells exhibited a severe hysteresis phenomenon with the HI of 16.89% due to its large amount of traps states in the film.

Conclusions

In summary, we reported an all-inorganic Nb incorporated $CsPbI_2Br$ perovskite for the first time. The Nb is incorporated into the perovskite lattice possibly by a slight substitution of Pb, which increases the perovskite tolerance factor and significantly stabilizes the α-$CsPbI_2Br$ phase. With 0.5% Nb incorporation, a high PCE of 10.42% was achieved for the carbon electrode based PSCs. The Nb incorporation has effectively reduced the charge recombination in the perovskite, resulting in high V_{oc} of 1.27 V and nearly hysteresis-free device. This work explicates the potential of the high-valence ions to serve as foreign ions to modify the properties of all-inorganic perovskite materials.

Acknowledgments

This work was supported by the Grant-in-Aid for Scientific Research (KAKENHI) program, Japan (C, Grant Number 15K05597), Takahashi Industrial and Economic Research Foundation (Takahashi Grant Number 06-003-154) and National Natural Science Foundation of China (Grant No. 51772039). The authors would like to thank the Research Center for Solar Light Energy Conversion, Kyushu Institute of Technology for their support. The computing work was carried out at LvLiang Cloud Computing Center of China, and the calculations were performed on TianHe-2.

Conflicts of Interests

There are no conflicts to declare.

Reference

1. Kojima, A.; Teshima, K.; Shirai, Y.; Miyasaka, T., Organometal halide perovskites as visible-light sensitizers for photovoltaic cells. *J. Am. Chem. Soc.* **2009,** *131* (17), 6050-6051.

2. https://www.nrel.gov/pv/assets/pdfs/pv-efficiency-chart.20190103.pdf.

3. Zhou, Y.; Yang, M.; Pang, S.; Zhu, K.; Padture, N. P., Exceptional morphology-preserving evolution of formamidinium lead triiodide perovskite thin films via organic-cation displacement. *J. Am. Chem. Soc.* **2016,** *138* (17), 5535-5538.

4. Kim, N.-K.; Min, Y. H.; Noh, S.; Cho, E.; Jeong, G.; Joo, M.; Ahn, S.-W.; Lee, J. S.; Kim, S.; Ihm, K., Investigation of Thermally Induced Degradation in $CH_3NH_3PbI_3$ Perovskite Solar Cells Using In-Situ Synchrotron Radiation Analysis. *Sci. Rep.* **2017,** *7* (1), 4645.

5. Zhou, G.; Wu, J.; Zhao, Y.; Li, Y.; Shi, J.; Li, Y.; Wu, H.; Li, D.; Luo, Y.; Meng, Q., Application of Cesium on the Restriction of Precursor Crystallization for Highly Reproducible Perovskite Solar Cells Exceeding 20% Efficiency. *ACS Appl. Mater. Inter.* **2018,** *10* (11), 9503-9513.

6. Park, N.-G.; Grätzel, M.; Miyasaka, T.; Zhu, K.; Emery, K., Towards stable and commercially available perovskite solar cells. *Nat. Energy* **2016,** *1* (11), 16152.

7. Nam, J. K.; Chun, D. H.; Rhee, R. J. K.; Lee, J. H.; Park, J. H., Methodologies toward Efficient and Stable Cesium Lead Halide Perovskite-Based Solar Cells. *Adv. Sci.* **2018**, 1800509.

8. Lin, J.; Lai, M.; Dou, L.; Kley, C. S.; Chen, H.; Peng, F.; Sun, J.; Lu, D.; Hawks, S. A.; Xie, C., Thermochromic halide perovskite solar cells. *Nat. Mater.* **2018,** *17* (3), 261.

9. Jena, A. K.; Kulkarni, A.; Sanehira, Y.; Ikegami, M.; Miyasaka, T., Stabilization of α-$CsPbI_3$ in Ambient Room Temperature Conditions by Incorporating Eu into $CsPbI_3$. *Chem. Mater.* **2018,** *30* (19), 6668-6674.

10. Xiang, W.; Wang, Z.; Kubicki, D. J.; Tress, W.; Luo, J.; Prochowicz, D.; Akin, S.; Emsley, L.; Zhou, J.; Dietler, G., Europium-Doped $CsPbI_2Br$ for Stable and Highly Efficient Inorganic Perovskite Solar Cells. *Joule* **2018,** *3*, 1-10.
11. Sutton, R. J.; Eperon, G. E.; Miranda, L.; Parrott, E. S.; Kamino, B. A.; Patel, J. B.; Hörantner, M. T.; Johnston, M. B.; Haghighirad, A. A.; Moore, D. T., Bandgap-tunable cesium lead halide perovskites with high thermal stability for efficient solar cells. *Adv. Energy Mater.* **2016,** *6* (8), 1502458.
12. Swarnkar, A.; Mir, W. J.; Nag, A., Can B-site doping or alloying improve thermal-and phase-stability of all-inorganic $CsPbX_3$ (X=Cl, Br, I) perovskites? *ACS Energy Lett.* **2018,** *3* (2), 286-289.
13. Zeng, Q.; Zhang, X.; Liu, C.; Feng, T.; Chen, Z.; Zhang, W.; Zheng, W.; Zhang, H.; Yang, B., Inorganic $CsPbI_2Br$ Perovskite Solar Cells: The Progress and Perspective. *Sol. RRL* **2018**, 1800239.
14. Zhou, Y.; Chen, J.; Bakr, O. M.; Sun, H.-T., Metal-Doped Lead Halide Perovskites: Synthesis, Properties, and Optoelectronic Applications. *Chem. Mater.* **2018,** *30* (19), 6589-6613.
15. Wu, X.; Luo, L.; Jiang, N.; Wu, X.; Zheng, Q., Effects of Nb doping on the microstructure, ferroelectric and piezoelectric properties of $0.7BiFeO_3$–$0.3BaTiO_3$ lead-free ceramics. *Bull. Mater. Sci.* **2016,** *39* (3), 737-742.
16. Yin, G.; Ma, J.; Jiang, H.; Li, J.; Yang, D.; Gao, F.; Zeng, J.; Liu, Z.; Liu, S. F., Enhancing efficiency and stability of perovskite solar cells through Nb-doping of TiO_2 at low temperature. *ACS Appl. Mater. Inter.* **2017,** *9* (12), 10752-10758.
17. Yuan, S.; Qian, F.; Yang, S.; Cai, Y.; Wang, Q.; Sun, J.; Liu, Z.; Liu, S., NbF_5: A Novel α-Phase Stabilizer for FA-Based Perovskite Solar Cells with High Efficiency. *Adv. Funct. Mater.* **2019**, 1807850.
18. Hu, Y.; Bai, F.; Liu, X.; Ji, Q.; Miao, X.; Qiu, T.; Zhang, S., Bismuth incorporation stabilized α-$CsPbI_3$ for fully inorganic perovskite solar cells. *ACS Energy Lett.* **2017,** *2* (10), 2219-2227.
19. Guo, Z.; Teo, S.; Xu, Z.; Zhang, C.; Kamata, Y.; Hayase, S.; Ma, T., Achievable high Voc of carbon based all-inorganic $CsPbIBr_2$ perovskite solar cells through interface engineering. *J. Mater. Chem. A* **2019,** *7*, 1227-1232.
20. Liu, C.; Li, W.; Zhang, C.; Ma, Y.; Fan, J.; Mai, Y., All-inorganic $CsPbI_2Br$ perovskite solar cells with high efficiency exceeding 13%. *J. Am. Chem. Soc.* **2018,** *140* (11), 3825-3828.
21. Wang, P.; Zhang, X.; Zhou, Y.; Jiang, Q.; Ye, Q.; Chu, Z.; Li, X.; Yang, X.; Yin, Z.; You, J., Solvent-controlled growth of inorganic perovskite films in dry environment for efficient and stable solar cells. *Nat. Commun.* **2018,** *9* (1), 2225.
22. Bai, D.; Zhang, J.; Jin, Z.; Bian, H.; Wang, K.; Wang, H.; Liang, L.; Wang, Q.; Liu, S. F., Interstitial Mn^{2+}-driven high-aspect-ratio grain growth for low-trap-density microcrystalline films for record efficiency $CsPbI_2Br$ solar cells. *ACS Energy Lett.* **2018,** *3* (4), 970-978.
23. Christodoulou, S.; Di Stasio, F.; Pradhan, S.; Stavrinadis, A.; Konstantatos, G., High-Open-Circuit-Voltage Solar Cells Based on Bright Mixed-Halide $CsPbBrI_2$ Perovskite Nanocrystals Synthesized under Ambient Air Conditions. *J. Phys. Chem. C* **2018,** *122* (14), 7621-7626.

24. Liang, J.; Liu, Z.; Qiu, L.; Hawash, Z.; Meng, L.; Wu, Z.; Jiang, Y.; Ono, L. K.; Qi, Y., Enhancing Optical, Electronic, Crystalline, and Morphological Properties of Cesium Lead Halide by Mn Substitution for High-Stability All-Inorganic Perovskite Solar Cells with Carbon Electrodes. *Adv. Energy Mater.* **2018**, 1800504.
25. Nam, J. K.; Chai, S. U.; Cha, W.; Choi, Y. J.; Kim, W.; Jung, M. S.; Kwon, J.; Kim, D.; Park, J. H., Potassium incorporation for enhanced performance and stability of fully inorganic cesium lead halide perovskite solar cells. *Nano Lett.* **2017,** *17* (3), 2028-2033.
26. Petrović, M.; Chellappan, V.; Ramakrishna, S., Perovskites: solar cells & engineering applications–materials and device developments. *Sol. Energy* **2015,** *122*, 678-699.
27. Dong, C.; Han, X.; Zhao, Y.; Li, J.; Chang, L.; Zhao, W., A Green Anti-Solvent Process for High Performance Carbon-Based $CsPbI_2Br$ All-Inorganic Perovskite Solar Cell. *Sol. RRL* **2018,** *2* (9), 1800139.
28. Liu, C.; Li, W.; Li, H.; Wang, H.; Zhang, C.; Yang, Y.; Gao, X.; Xue, Q.; Yip, H. L.; Fan, J., Structurally Reconstructed $CsPbI_2Br$ Perovskite for Highly Stable and Square-Centimeter All-Inorganic Perovskite Solar Cells. *Adv. Energy Mater.* **2018**, 1803572.
29. You, P.; Liu, Z.; Tai, Q.; Liu, S.; Yan, F., Efficient semitransparent perovskite solar cells with graphene electrodes. *Adv. Mater.* **2015,** *27* (24), 3632-3638.
30. Zhang, J.; Shang, M.-h.; Wang, P.; Huang, X.; Xu, J.; Hu, Z.; Zhu, Y.; Han, L., n-Type Doping and Energy States Tuning in $CH_3NH_3Pb_{1-x}Sb_{2x/3}I_3$ Perovskite Solar Cells. *ACS Energy Lett.* **2016,** *1* (3), 535-541.
31. Li, Z.; Yang, M.; Park, J.-S.; Wei, S.-H.; Berry, J. J.; Zhu, K., Stabilizing perovskite structures by tuning tolerance factor: formation of formamidinium and cesium lead iodide solid-state alloys. *Chem. Mater.* **2015,** *28* (1), 284-292.
32. Guo, Z.; Gao, L.; Xu, Z.; Teo, S.; Zhang, C.; Kamata, Y.; Hayase, S.; Ma, T., High Electrical Conductivity 2D MXene Serves as Additive of Perovskite for Efficient Solar Cells. *Small* **2018,** *14* (47), 1802738.
33. Zuo, C.; Ding, L., An 80.11% FF record achieved for perovskite solar cells by using the NH_4Cl additive. *Nanoscale* **2014,** *6* (17), 9935-9938.
34. Ma, J.; Yang, G.; Qin, M.; Zheng, X.; Lei, H.; Chen, C.; Chen, Z.; Guo, Y.; Han, H.; Zhao, X., MgO Nanoparticle Modified Anode for Highly Efficient SnO_2-Based Planar Perovskite Solar Cells. *Adv. Sci.* **2017,** *4* (9), 1700031.
35. Hou, Y.; Chen, X.; Yang, S.; Li, C.; Zhao, H.; Yang, H. G., A Band-Edge Potential Gradient Heterostructure to Enhance Electron Extraction Efficiency of the Electron Transport Layer in High-Performance Perovskite Solar Cells. *Adv. Funct. Mater.* **2017,** *27* (27), 1700878.
36. Yang, F.; Hirotani, D.; Kapil, G.; Kamarudin, M. A.; Ng, C. H.; Zhang, Y.; Shen, Q.; Hayase, S., All-Inorganic $CsPb_{1-x}Ge_xI_2Br$ Perovskite with Enhanced Phase Stability and Photovoltaic Performance. *Angew. Chem. Int. Ed.* **2018,** *57* (39), 12745-12749.
37. Zhao, W.; Yao, Z.; Yu, F.; Yang, D.; Liu, S., Alkali Metal Doping for Improved $CH_3NH_3PbI_3$ Perovskite Solar Cells. *Adv. Sci.* **2018,** *5* (2), 1700131.

38. Zhao, W.; Yang, D.; Yang, Z.; Liu, S. F., Zn-doping for reduced hysteresis and improved performance of methylammonium lead iodide perovskite hybrid solar cells. *Mater. Today Energy* **2017,** *5*, 205-213.
39. Xiang, S.; Li, W.; Wei, Y.; Liu, J.; Liu, H.; Zhu, L.; Chen, H., The synergistic effect of non-stoichiometry and Sb-doping on air-stable α-$CsPbI_3$ for efficient carbon-based perovskite solar cells. *Nanoscale* **2018,** *10*, 9996-10004
40. Chen, Q.; Chen, L.; Ye, F.; Zhao, T.; Tang, F.; Rajagopal, A.; Jiang, Z.; Jiang, S.; Jen, A. K.-Y.; Xie, Y., Ag-incorporated organic–inorganic perovskite films and planar heterojunction solar cells. *Nano Lett.* **2017,** *17*, 3231-3237.
41. Dong, Q.; Wang, Z.; Zhang, K.; Yu, H.; Huang, P.; Liu, X.; Zhou, Y.; Chen, N.; Song, B., Easily accessible polymer additives for tuning the crystal-growth of perovskite thin-films for highly efficient solar cells. *Nanoscale* **2016,** *8*, 5552-5558.
42. Hadadian, M.; Correa-Baena, J. P.; Goharshadi, E. K.; Ummadisingu, A.; Seo, J. Y.; Luo, J.; Gholipour, S.; Zakeeruddin, S. M.; Saliba, M.; Abate, A., Enhancing Efficiency of Perovskite Solar Cells via N-doped Graphene: Crystal Modification and Surface Passivation. *Adv. Mater.* **2016,** *28*, 8681-8686.
43. Li, W.; Rothmann, M. U.; Liu, A.; Wang, Z.; Zhang, Y.; Pascoe, A. R.; Lu, J.; Jiang, L.; Chen, Y.; Huang, F., Phase segregation enhanced ion movement in efficient inorganic $CsPbIBr_2$ solar cells. *Adv. Energy Mater.* **2017,** *7* (20), 1700946.
44. Lee, J.-W.; Kim, S.-G.; Bae, S.-H.; Lee, D.-K.; Lin, O.; Yang, Y.; Park, N.-G., The interplay between trap density and hysteresis in planar heterojunction perovskite solar cells. *Nano Lett.* **2017,** *17* (7), 4270-4276.